

# Volumetric heat capacity and capillary pressure fractal dimensions for characterizing shajara reservoirs of the permo-carboniferous shajara formation, Saudi Arabia

Khalid Elyas Mohamed Elameen Alkhidir\*

Department of Petroleum and Natural Gas Engineering, College of Engineering, King Saud University, Saudi Arabia

## Abstract

The quality and assessment of a reservoir can be documented in detail by the application of volumetric heat capacity. This research aims to calculate fractal dimension from the relationship among volumetric heat capacity, maximum volumetric heat capacity and wetting phase saturation and to approve it by the fractal dimension derived from the relationship among capillary pressure and wetting phase saturation. Two equations for calculating the fractal dimensions have been employed. The first one describes the functional relationship between wetting phase saturation, volumetric heat capacity, maximum volumetric heat capacity and fractal dimension. The second equation implies to the wetting phase saturation as a function of capillary pressure and the fractal dimension. Two procedures for obtaining the fractal dimension have been utilized. The first procedure was done by plotting the logarithm of the ratio between volumetric heat capacity and maximum volumetric heat capacity versus logarithm wetting phase saturation. The slope of the first procedure = 3-Df (fractal dimension). The second procedure for obtaining the fractal dimension was determined by plotting the logarithm of capillary pressure versus the logarithm of wetting phase saturation. The slope of the second procedure = Df - 3. On the basis of the obtained results of the fabricated stratigraphic column and the attained values of the fractal dimension, the sandstones of the Shajara reservoirs of the Shajara Formation were divided here into three units.

## Introduction

Seismo electric effects related to electro kinetic potential, dielectric permittivity, pressure gradient, fluid viscosity, and electric conductivity was first reported by [1]. Capillary pressure follows the scaling law at low wetting phase saturation was reported by [2]. Seismo electric phenomenon by considering electro kinetic coupling coefficient as a function of effective charge density, permeability, fluid viscosity and electric conductivity was reported by [3]. The magnitude of seismo electric current depends on porosity, pore size, zeta potential of the pore surfaces, and elastic properties of the matrix was investigated by [4]. The tangent of the ratio of converted electric field to pressure is approximately in inverse proportion to permeability was studied by [5]. Permeability inversion from seismo electric log at low frequency was studied by [6]. They reported that, the tangent of the ratio among electric excitation intensity and pressure field is a function of porosity, fluid viscosity, frequency, tortuosity, fluid density and Dracy permeability. A decrease of seismo electric frequencies with increasing water content was reported by [7]. An increase of seismo electric transfer function with increasing water saturation was studied by [8]. An increase of dynamic seismo electric transfer function with decreasing fluid conductivity was described by [9]. The amplitude of seismo electric signal increases with increasing permeability which means that the seismo electric effects are directly related to the permeability and can be used to study the permeability of the reservoir was illustrated by [10]. Seismo electric coupling is frequency dependent and decreases exponentially when frequency increases was demonstrated by [11]. An increase of permeability with increasing pressure head and bubble pressure fractal dimension was reported by [12,13]. An increase of geometric relaxation time of induced polarization fractal dimension with permeability increasing and grain size was described by [14,15].

## Materials and methods

Sandstone samples were collected from the surface type section of the Permo-Carboniferous Shajara Formation, latitude 26° 52' 17.4", longitude 43° 36' 18" (Figure 1). Porosity was measured on collected samples using mercury intrusion Porosimetry and permeability was derived from capillary pressure data. The purpose of this paper is to obtain volumetric heat capacity fractal dimension and to confirm it by capillary pressure fractal dimension. The fractal dimension of the first procedure is determined from the positive slope of the plot of logarithm of the ratio of volumetric heat capacity to maximum volumetric heat capacity  $\log(VHC^{1/2}/VHC_{max}^{1/2})$  versus  $\log$  wetting phase saturation ( $\log Sw$ ). Whereas the fractal dimension of the second procedure is determined from the negative slope of the plot of logarithm of capillary pressure ( $\log Pc$ ) versus logarithm of wetting phase saturation ( $\log Sw$ ).

The volumetric heat capacity can be scaled as,

$$S_w = \left[ \frac{VHC^{1/2}}{VHC_{max}^{1/2}} \right]^{-[3-Df]} \quad 1$$

Where  $S_w$  the water saturation,  $VHC$  the volumetric heat capacity in Joule / kelvin \* cubic meter,  $VHC_{max}$  the maximum volumetric heat capacity in Joule / kelvin \* cubic meter, and  $Df$  the fractal dimension.

\*Correspondence to: Khalid Elyas Mohamed Elameen Alkhidir, Department of Petroleum and Natural Gas Engineering, College of Engineering, King Saud University, Saudi Arabia, E-mail: kalkhidir@ksu.edu.sa

**Key words:** shajara reservoirs, shajara formation, volumetric heat capacity fractal dimension, capillary pressure fractal dimension

**Received:** July 17, 2019; **Accepted:** July 22, 2019; **Published:** July 29, 2019

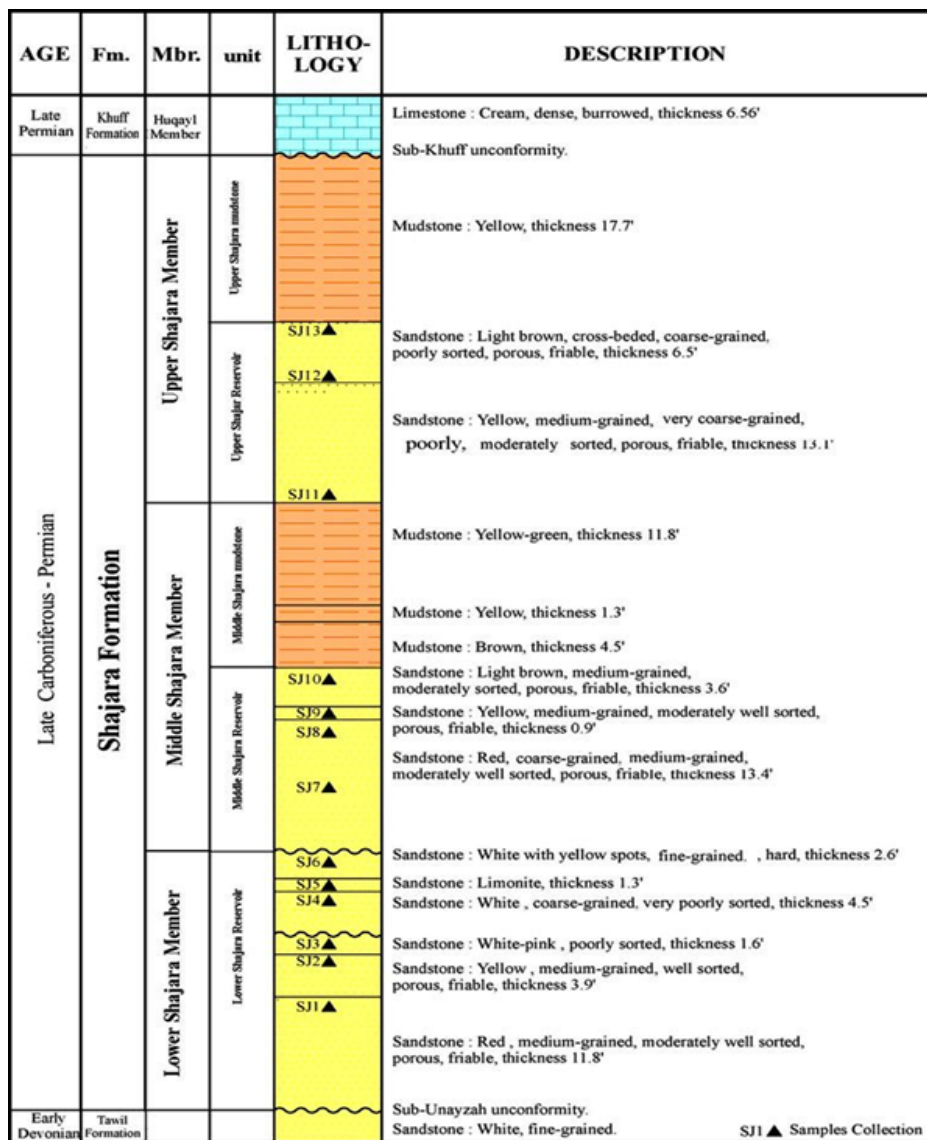


Figure 1. Surface type section of the Shajara Reservoirs of the Permo-Carboniferous Shajara Formation at latitude 26° 52' 17.4" longitude 43° 36' 18"

Equation 1 can be proofed from

$$Q = \Delta T * Vol * VHC \tag{2}$$

Where Q the heat in Joule,  $\Delta T$  temperature difference in kelvin, Vol the volume in cubic meter, VHC the volumetric heat capacity in Joule / kelvin \* cubic meter.

The volume Vol can be scaled as

$$Vol = \left[ \frac{m}{\rho} \right] \tag{3}$$

Where Vol the volume in cubic meter, m the mass in kilo gram,  $\rho$  the density in kilo gram/cubic meter

Insert equation 3 into equation 2

$$Q = \left[ \frac{\Delta T * m * VHC}{\rho} \right] \tag{4}$$

The mass m can be scaled as

$$m = \left[ \frac{F}{g} \right] \tag{5}$$

Where m the mass in kilo gram, F the force in Newton, g acceleration in meter/square second

Insert equation 5 into equation 4

$$Q = \left[ \frac{\Delta T * F * VHC}{\rho * g} \right] \tag{6}$$

The acceleration g can be scaled as

$$g = \left[ \frac{E}{\psi} \right] \tag{7}$$

Where g the acceleration in meter/square second, E the electric field in volt/meter,  $\psi$  the electric transfer function in volt \* square second/square meter.

Insert equation 7 into equation 6

$$Q = \left[ \frac{\Delta T * F * VHC * \psi}{\rho * E} \right] \quad 8$$

The electric field E can be scaled as

$$E = \left[ \frac{V}{CEK} \right] \quad 9$$

Where E the electric field in volt / meter, V the velocity in meter/ second, CEK the electro kinetic coefficient in ampere / pascal \* meter

Insert equation 9 into equation 8

$$Q = \left[ \frac{\Delta T * F * VHC * \psi * CEK}{\rho * V} \right] \quad 10$$

The velocity V can be scaled as

$$V = \left[ \frac{Q'}{A} \right] \quad 11$$

Where V the velocity in meter / second, Q' the flow rate in cubic meter / second, A the area in square meter

Insert equation 11 into equation 10

$$Q = \left[ \frac{\Delta T * F * VHC * \psi * CEK * A}{\rho * Q'} \right] \quad 12$$

Equation 12 after rearrange will become

$$Q * Q' = \left[ \frac{\Delta T * F * VHC * \psi * CEK * A}{\rho} \right] \quad 13$$

The flow rate Q' can be scaled as

$$Q' = \left[ \frac{k * A * \Delta P}{\mu * L} \right] \quad 14$$

Where Q' the flow rate in cubic meter / second, k the permeability in square meter, A the area in square meter, ΔP the differential pressure in pascal, μ the fluid viscosity in pascal second, L the capillary length in meter.

Insert equation 14 into equation 13

$$Q * K * A * \Delta P = \left[ \frac{\Delta T * F * VHC * \psi * CEK * A * \mu * L}{\rho} \right] \quad 15$$

The maximum permeability  $k_{max}$  can be scaled as

$$Q * K_{max} * A * \Delta P = \left[ \frac{\Delta T * F * VHC_{max} * \psi * CEK * A * \mu * L}{\rho} \right] \quad 16$$

Divide equation 15 by equation 16

$$\left[ \frac{Q * K * A * \Delta P}{Q * K_{max} * A * \Delta P} \right] = \left[ \frac{\left[ \frac{\Delta T * F * VHC * \psi * CEK * A * \mu * L}{\rho} \right]}{\left[ \frac{\Delta T * F * VHC_{max} * \psi * CEK * A * \mu * L}{\rho} \right]} \right] \quad 17$$

Equation 17 after simplification will become

$$\left[ \frac{K}{K_{max}} \right] = \left[ \frac{VHC}{VHC_{max}} \right] \quad 18$$

Take the square root of equation 18

$$\sqrt{\left[ \frac{K}{K_{max}} \right]} = \sqrt{\left[ \frac{VHC}{VHC_{max}} \right]} \quad 19$$

Equation 19 after simplification will become

$$\left[ \frac{K^{\frac{1}{2}}}{K_{max}^{\frac{1}{2}}} \right] = \left[ \frac{VHC^{\frac{1}{2}}}{VHC_{max}^{\frac{1}{2}}} \right] \quad 20$$

$$\text{But; } \left[ \frac{K^{\frac{1}{2}}}{K_{max}^{\frac{1}{2}}} \right] = \left[ \frac{VHC^{\frac{1}{2}}}{VHC_{max}^{\frac{1}{2}}} \right] = \left[ \frac{r}{r_{max}} \right] \quad 21$$

Where r the pore radius in meter,  $r_{max}$  the maximum pore radius in meter

Take the logarithm of equation 21

$$\log \left[ \frac{K^{\frac{1}{2}}}{K_{max}^{\frac{1}{2}}} \right] = \log \left[ \frac{VHC^{\frac{1}{2}}}{VHC_{max}^{\frac{1}{2}}} \right] = \log \left[ \frac{r}{r_{max}} \right] \quad 22$$

$$\text{But; } \log \left[ \frac{r}{r_{max}} \right] = \left[ \frac{\log S_w}{3 - Df} \right] \quad 23$$

Insert equation 23 into equation 22

$$\left[ \frac{\log S_w}{3 - Df} \right] = \log \left[ \frac{VHC^{\frac{1}{2}}}{VHC_{max}^{\frac{1}{2}}} \right] \quad 24$$

Equation 24 after log removal will become

$$S_w = \left[ \frac{VHC^{\frac{1}{2}}}{VHC_{max}^{\frac{1}{2}}} \right]^{3 - Df} \quad 25$$

Equation 25 the proof of equation 1 which relates the water saturation, volumetric heat capacity, maximum volumetric heat capacity and the fractal dimension.

The capillary pressure can be scaled as

$$\log S_w = [Df - 3] * \log Pc + \text{constant} \quad 26$$

Where Sw the water saturation, Pc the capillary pressure and Df the fractal dimension.

## Results and discussion

Based on field observation the Shajara Reservoirs of the Permo-Carboniferous Shajara Formation were divided here into three units as described in Figure 1. These units from bottom to top are: Lower Shajara Reservoir, Middle Shajara reservoir, and Upper Shajara Reservoir. Their attained results of the volumetric heat capacity fractal dimension and capillary pressure fractal dimension are shown in Table 1. Based on the achieved results it was found that the volumetric heat capacity fractal dimension is equal to the capillary pressure fractal dimension. The maximum value of the fractal dimension was found to be 2.7872 allocated to sample SJ13 from the Upper Shajara Reservoir as verified in Table 1. Whereas the minimum value of the fractal dimension 2.4379 was reported from sample SJ3 from the Lower Shajara reservoir as

shown in Table 1. The Volumetric heat capacity fractal dimension and capillary pressure fractal dimension were detected to increase with increasing permeability as proved in Table 1 owing to the possibility of having interconnected channels.

The Lower Shajara reservoir was symbolized by six sandstone samples (Figure 1), four of which label as SJ1, SJ2, SJ3 and SJ4 were carefully chosen for capillary pressure measurement as proven in Table 1. Their positive slopes of the first procedure log of the Volumetric heat capacity to maximum Volumetric heat capacity *versus* log wetting phase saturation (Sw) and negative slopes of the second procedure log capillary pressure (Pc) *versus* log wetting phase saturation (Sw) are clarified in Figures 2-5 and Table 1. Their Volumetric heat capacity fractal dimension and capillary pressure fractal dimension values are revealed in Table 1. As we proceed from sample SJ2 to SJ3 a pronounced reduction in permeability due to compaction was described from 1955 md to 56 md which reflects decrease in Volumetric heat capacity fractal dimension from 2.7748 to 2.4379 as quantified in Table 1. Again, an increase in grain size and permeability was proved from sample SJ4 whose volumetric heat capacity fractal dimension and capillary pressure fractal dimension was found to be 2.6843 as described in Table 1.

In contrast, the Middle Shajara reservoir which is separated from the Lower Shajara reservoir by an unconformity surface as revealed in Figure 1. It was nominated by four samples (Figure 1), three of which named as SJ7, SJ8, and SJ9 as illuminated in Table 1 were chosen for capillary measurements as described in Table 1. Their positive slopes

of the first procedure and negative slopes of the second procedure are shown in Figures 6-8 and Table 1. Furthermore, their Volumetric heat capacity fractal dimensions and capillary pressure fractal dimensions show similarities as defined in Table 1. Their fractal dimensions are higher than those of samples SJ3 and SJ4 from the Lower Shajara Reservoir due to an increase in their permeability as explained in Table 1.

On the other hand, the Upper Shajara reservoir was separated from the Middle Shajara reservoir by yellow green mudstone as shown in Figure 1. It is defined by three samples so called SJ11, SJ12, SJ13 as explained in Table 1. Their positive slopes of the first procedure and negative slopes of the second procedure are displayed in Figures 9-11 and Table 1. Moreover, their volumetric heat capacity fractal dimension and capillary pressure fractal dimension are also higher than those of sample SJ3 and SJ4 from the Lower Shajara Reservoir due to an increase in their permeability as simplified in Table 1.

Overall a plot of positive slope of the first procedure versus negative slope of the second procedure as described in Figure 12 reveals three permeable zones of varying Petrophysical properties. These reservoir zones were also confirmed by plotting volumetric heat capacity fractal dimension versus capillary pressure fractal dimension as described in Figure 13. Such variation in fractal dimension can account for heterogeneity which is a key parameter in reservoir quality assessment.

**Table 1.** Petrophysical model showing the three Shajara Reservoir Units with their corresponding values of Volumetric heat capacity fractal dimension and capillary pressure fractal dimension

Formation	Reservoir	Sample	Porosity %	k (md)	Positive slope of the first procedure Slope=3-Df	Negative slope of the second procedure Slope=Df-3	Volumetric heat capacity fractal dimension	Capillary pressure fractal dimension
Permo-Carboniferous Shajara Formation	Upper Shajara Reservoir	SJ13	25	973	0.2128	-0.2128	2.7872	2.7872
		SJ12	28	1440	0.2141	-0.2141	2.7859	2.7859
		SJ11	36	1197	0.2414	-0.2414	2.7586	2.7586
	Middle Shajara Reservoir	SJ9	31	1394	0.2214	-0.2214	2.7786	2.7786
		SJ8	32	1344	0.2248	-0.2248	2.7752	2.7752
		SJ7	35	1472	0.2317	-0.2317	2.7683	2.7683
	Lower Shajara Reservoir	SJ4	30	176	0.3157	-0.3157	2.6843	2.6843
		SJ3	34	56	0.5621	-0.5621	2.4379	2.4379
		SJ2	35	1955	0.2252	-0.2252	2.7748	2.7748
		SJ1	29	1680	0.2141	-0.2141	2.7859	2.7859

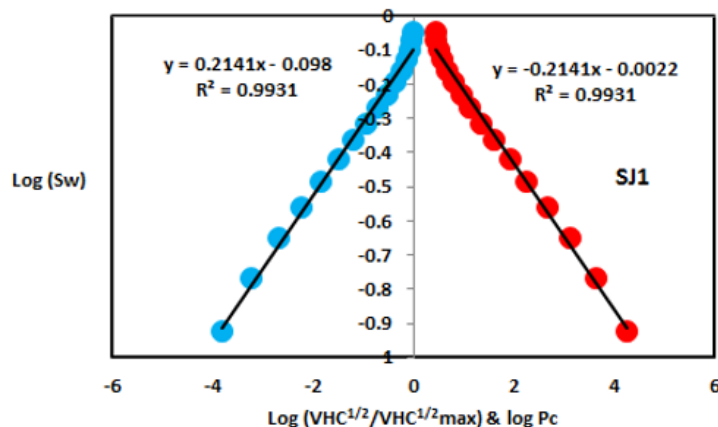


**Figure 2.** Log (VHC1/2/VHC1/2max) & log pc *versus* log Sw for sample SJ1

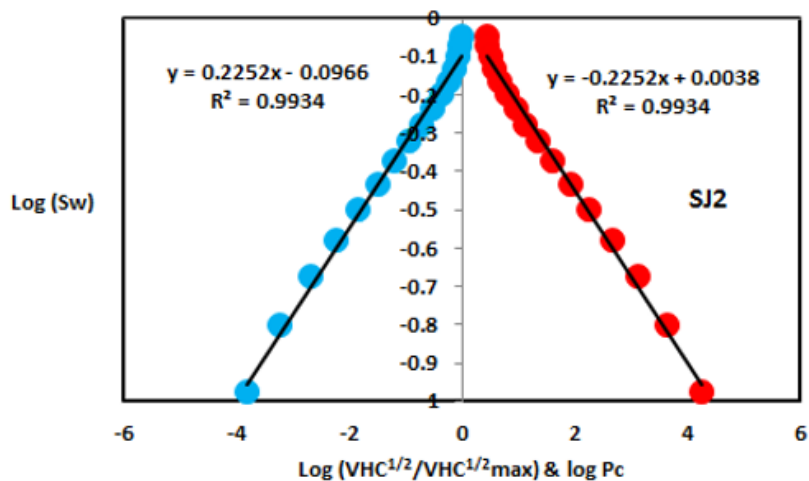


Figure 3. Log (VHC1/2/VHC1/2max) & log pc versus log Sw for sample SJ2

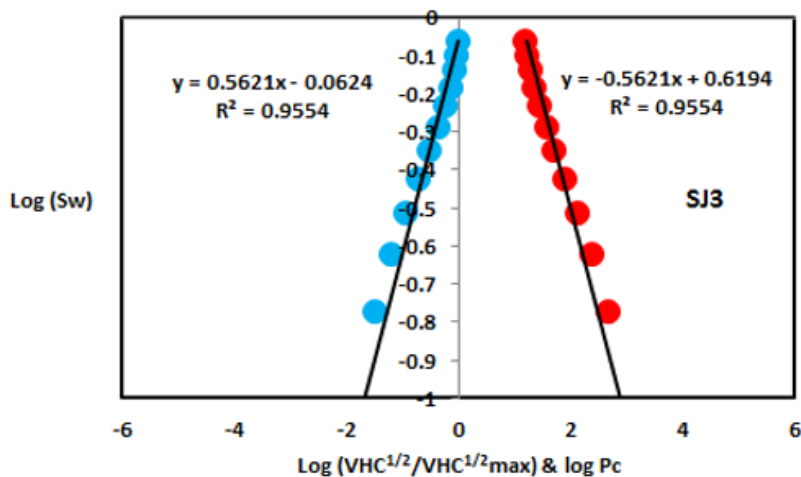


Figure 4. Log (VHC1/2/VHC1/2max) & log pc versus log Sw for sample SJ3

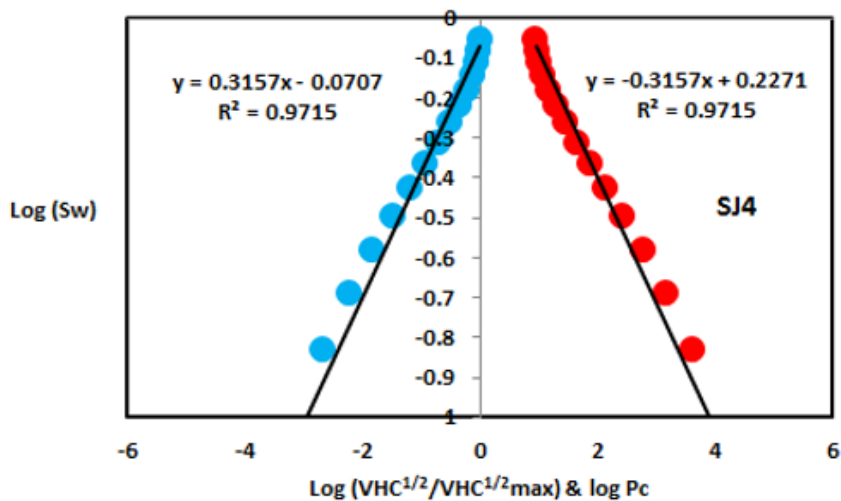


Figure 5. Log (VHC1/2/VHC1/2max) & log pc versus log Sw for sample SJ4

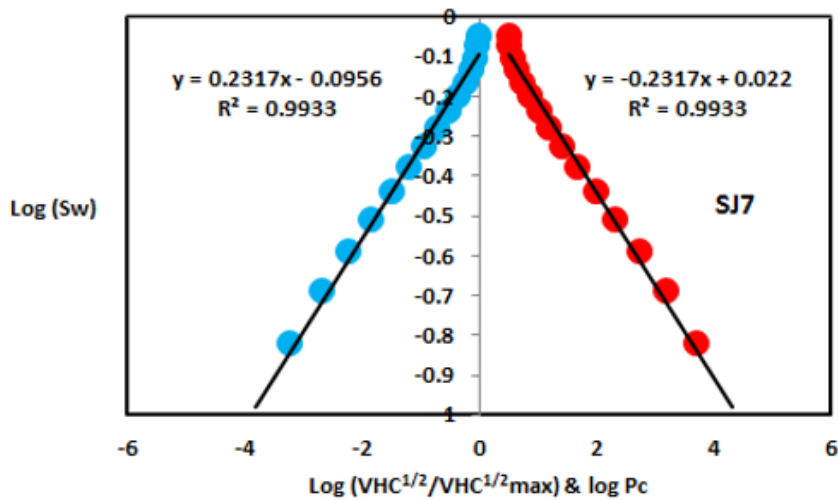


Figure 6. Log (VHC1/2/VHC1/2max) & log pc versus log Sw for sample SJ7

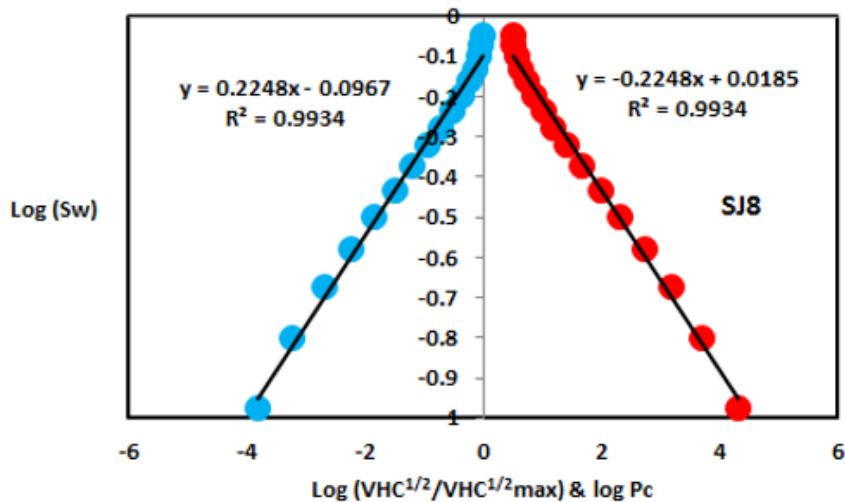


Figure 7. Log (VHC1/2/VHC1/2max) & log pc versus log Sw for sample SJ8

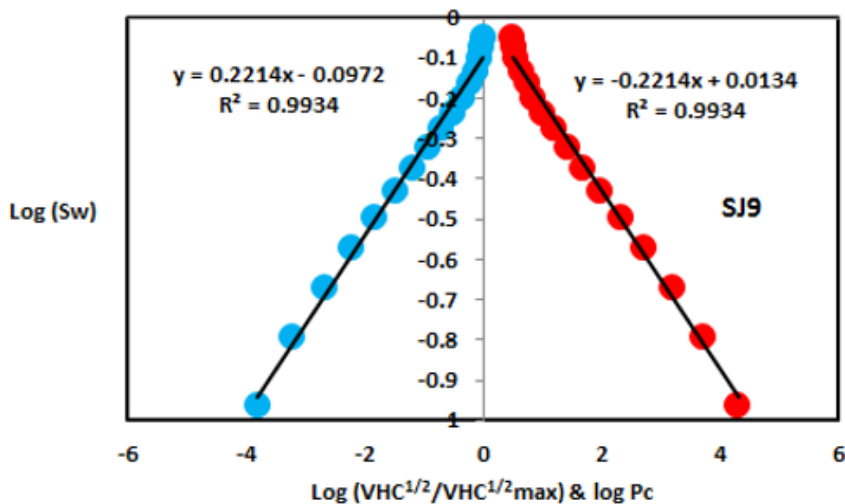


Figure 8. Log (VHC1/2/VHC1/2max) & log pc versus log Sw for sample SJ9

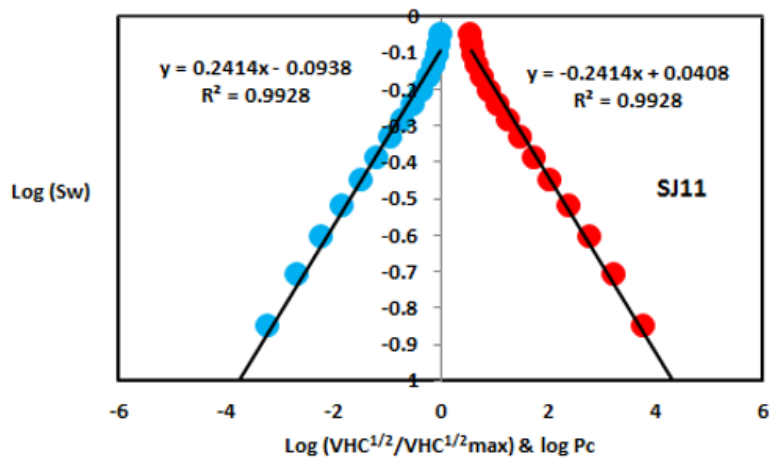


Figure 9. Log (VHC1/2/VHC1/2max) & log pc versus log Sw for sample SJ11

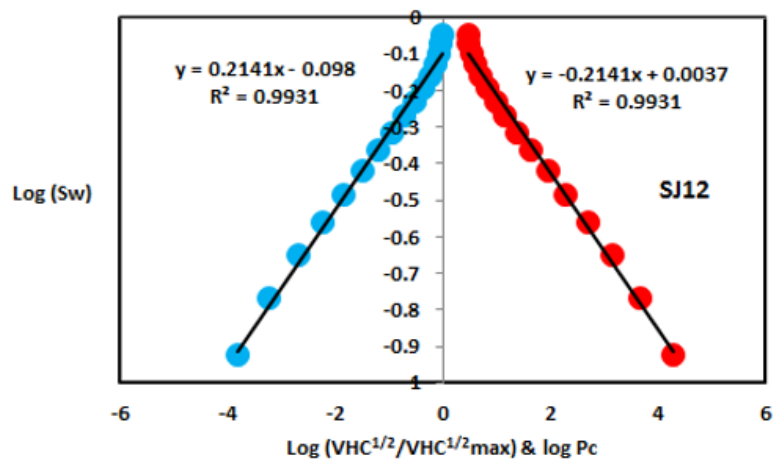


Figure 10. Log (VHC1/2/VHC1/2max) & log pc versus log Sw for sample SJ12

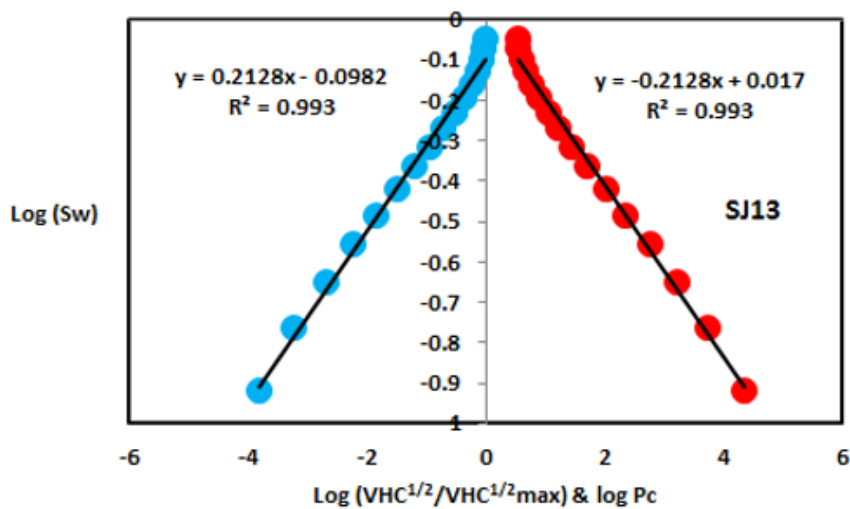


Figure 11. Log (VHC1/2/VHC1/2max) & log pc versus log Sw for sample SJ13

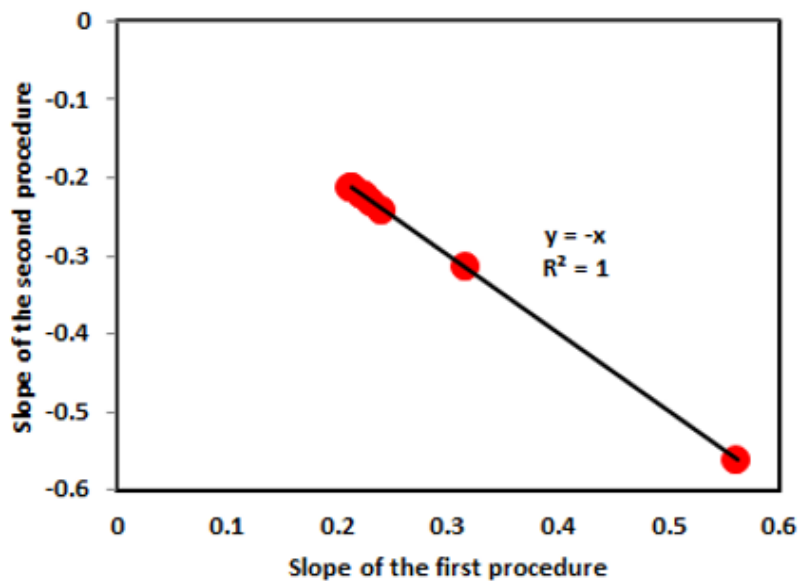


Figure 12. Slope of the first procedure versus slope of the second procedure

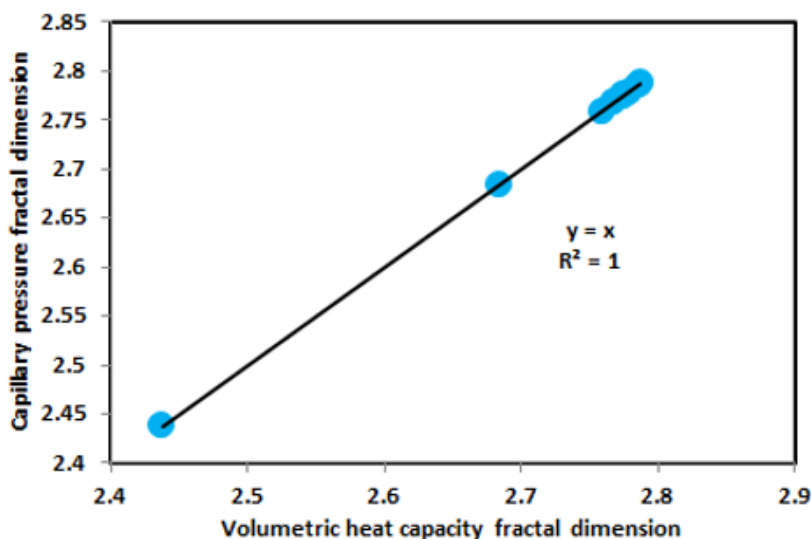


Figure 13. Volumetric heat capacity fractal dimension versus capillary pressure fractal dimension

## Conclusion

The sandstones of the Shajara Reservoirs of the permo-Carboniferous Shajara Formation were divided here into three units based on volumetric heat capacity fractal dimension. The Units from base to top are: Lower Shajara Volumetric Heat Capacity Fractal Dimension Unit, Middle Shajara Volumetric Heat Capacity Fractal Dimension Unit, and Upper Shajara Volumetric Heat Capacity Fractal Dimension Unit. These units were also proved by capillary pressure fractal dimension. The fractal dimension was found to increase with increasing grain size and permeability owing to possibility of having interconnected channels.

## Acknowledgement

The author would to thank King Saud University, College of Engineering, Department of Petroleum and Natural Gas Engineering, Department of Chemical Engineering, Research Centre at College

of Engineering, College of Science, Department of Geology and Geophysics, and King Abdullah Institute for research and Consulting Studies for their supports.

## References

1. Frenkel J (1944) On the theory of seismic and seismoelectric phenomena in a moist soil. *J phys* 3: 230-241.
2. Li K, Williams W (2007) Determination of capillary pressure function from resistivity data. *Trans Porous Media* 67: 1-15.
3. Revil A, Jardani A (2010) Seismoelectric response of heavy oil reservoirs: theory and numerical modelling. *Geophys J Int* 180: 781-797.
4. Dukhin A, Goetz P, Thommes M (2010) Seismoelectric effect: a non-isochoric streaming current.1 Experiment. *J Colloid Interface Sci* 345: 547-553. [Crossref]
5. Guan W, Hu H, Wang Z (2012) Permeability inversion from low-frequency seismoelectric logs in fluid- saturated porous formations. *Geophys Prospect* 61: 120-133.
6. Hu H, Guan W, Zhao W (2012) Theoretical studies of permeability inversion from seismoelectric logs. *Geophys Res Abs* 14: EGU2012-6725-1.



7. Borde C, Senechal P, Barriere J, Brito D, Normandin et al. (2015) Impact of water saturation on seismoelectric transfer functions: a laboratory study of co-seismic phenomenon. *Geophys J Int* 200: 1317-1335.
8. Jardani A, Revil A (2015) Seismoelectric couplings in a poroelastic material containing two immiscible fluid phases. *Geophys J Int* 202: 850-870.
9. Holzhauer J, Brito D, Bordes C, Brun Y, Guatarbes B, et al. (2016) Experimental quantification of the seismoelectric transfer function and its dependence on conductivity and saturation in loose sand. *Geophys Prospect* 65: 1097-1120.
10. Ping R, Wei JX, Di BR, Ding PB, Liu ZC, et al. (2016) Experimental research on seismoelectric effects in sandstone. *Appl Geophys* 13: 425-436.
11. Djuraev U, Jufar SR, Vasant P (2017) Numerical Study of frequency-dependent seismo electric coupling in partially-saturated porous media. MATEC Web of Conferences.
12. Al-khidir KEME (2017) Pressure head fractal dimension for characterizing Shajara Reservoirs of the Shajara Formation of the Permo-Carboniferous Unayzah Group, Saudi Arabia. *Arch Pet Environ Biotechnol* 2: 1-7.
13. Al-Khidir KE (2018) On Similarity of Pressure Head and Bubble Pressure Fractal Dimensions for Characterizing Permo-Carboniferous Shajara Formation, Saudi Arabia. *J Indust Pollut oxie* 1: 1-10.
14. Al-khidir KEME (2018) Geometric relaxation time of induced polarization fractal dimension for characterizing Shajara Reservoirs of the Shajara Formation of the Permo-Carboniferous Unayzah Group, Saudi Arabia. *SF J Petrol* 2: 1-6.
15. Alkhidir KEME (2018) Geometric relaxation time of induced polarization fractal dimension for characterizing Shajara Reservoirs of the Shajara formation of the Permo-Carboniferous Unayzah Group-Permo. *Int J Pet Res* 2: 105-108.